

Impact of Pore Size and Morphology of Porous Organosilicate Glasses on Integrated Circuit Manufacturing

Mark L O'Neill¹, Mary K Haas¹, Brian K Peterson², Raymond N Vrtis¹, Scott J Weigel¹, Dingjun Wu¹, Mark D Bitner¹, and Eugene J Karwacki¹

¹Electronics Technology, Air Products & Chemicals, Inc, 7201 Hamilton Blvd., Allentown, PA, 18195

²Computational Modeling Center, Air Products & Chemicals, Inc, 7201 Hamilton Blvd., Allentown, PA, 18195

ABSTRACT

Porous organosilicate materials produced by plasma enhanced chemical vapor deposition are the leading candidates for back-end-of-line dielectric insulators for IC manufacturing at 45nm design features and beyond. The properties of porous organosilicate glass films of dielectric constant $k=2.50 \pm 0.05$ formed using diethoxymethylsilane and five different porogen precursors with an ultraviolet post treatment are reported. By varying the porogen precursor type pore sizes of 1-2 nm (equivalent spherical diameter) and porosities in the range of 24-31% were measured. While there were no observable trends in pore size with the molecular volume or plasma reactivity of the porogen precursor, modulus values ranged from 6.6 to 10.8 GPa. Porous films with the highest mechanical properties were found to have the highest matrix dielectric constant, highest network connectivity (lowest methyl content), and highest density. Within this process space, maximizing the network connectivity of the film was found to be more important to mechanical properties than lowering the total porosity. In effect, the choice of porogen precursor dictates the film morphology through its impact on the organosilicate glass matrix and pore size.

INTRODUCTION

Materials with increasingly lower dielectric constant values are needed for future generation integrated circuits (ICs) in order to continue to enhance signal propagation. Current state of the art IC production uses organosilicate glasses (OSGs) with dielectric constant (k) values on the order of 3.0. Dense OSG materials, however, are inherently limited to k values ≥ 2.7 [1-3]. To achieve k values of < 2.5 alternative materials, processing, or a combination of both must be used.

The introduction of porosity is one commonly used technique to reduce dielectric constant, where the degree of reduction depends largely upon the film porosity. While porous materials inherently suffer from inferior mechanical properties relative to their non-porous predecessors, post-treatment processes such as UV and e-beam can dramatically improve the integratability of these materials. It is known that a variety of organosilane / organosiloxane precursors can be used to produce OSG films by chemical vapor deposition (CVD) with acceptable mechanical properties [1, 2, 4-7]. It has been shown in previous studies [1, 8] the benefits of diethoxymethylsilane (DEMSTTM ILD precursor) as a precursor for interlayer/intermetal dielectric films in providing an excellent balance of electrical and mechanical properties for a methyl-doped silicate glass. Porous OSG materials produced by plasma enhanced chemical vapor deposition have arisen as the leading candidates for back-end-of-line dielectric insulators for 45nm generation IC manufacturing. The PDEMSTTM ILD process [9] utilizes an OSG precursor and an organic porogen precursor to deposit an OSG-organic composite film. The labile organic

material in the film functions as a porogen, occupying space within the matrix during the film formation phase. The composite (aka. as-deposited) film may be treated with various post-treatment processes such as thermal, visible/ultraviolet radiation, and electron beams to produce pores and mechanically fortify the structure.

The interactions of subsequent process steps used in back-end-of-line (BEOL) processing of interconnect structures with porous ILD materials is the focus of much study. Porous organosilicate glasses produced from the combination of diethoxymethylsilane (DEMS® ILD precursor) and organic porogen precursors have been shown to produce films with k values < 2.0 with monodisperse porosity centered around 1.5-1.7 nm in diameter [10]. It will be shown how the porogen precursor can impact film properties, pore size, and the morphology of the film, and the potential relevance this has on the integration of these films into interconnect structures.

EXPERIMENTAL

All depositions were performed on an Applied Materials Precision 5000 in a 200mm DxZ chamber fitted with a TEOS-oxide process kit. Temperature, pressure, chemical flow, electrode spacing, carrier gas flow and type, and plasma power were optimized for each formulation in attempts to achieve the best combination of electrical and mechanical properties. For the films tested here the process window for all depositions involving porogen precursors were 275-300 °C, 8 torr, 0.35" gap between the substrate and showerhead/electrode, 200 sccm CO₂ carrier, 0-25 sccm oxygen, 600-750 Watts rf (single frequency, 13.56 MHz), and total chemical flow 700-900 mg/min. The ratio of diethoxymethylsilane to porogen precursor (aka. formulation) used for each deposition was tailored to achieve the desired final dielectric constant value.

All as-deposited PDEMS[#] films employing porogen precursors were treated by exposure to a Fusion H+ ultraviolet lamp (model I-600) in order to render them porous. Exposures were performed with the Fusion lamp system retrofitted onto an Applied P-5000 DxL chamber; the chamber was modified by replacing the standard lid with a synthetic silica window to allow for transmission of radiation. The bulb was positioned in the reflector to provide collimated UV light with an approximate exposure region of 2" x 10". The UV bulb was cycled horizontally across the surface of the film at a rate of approximately 10 seconds per cycle with the wafer held at approximately 400 °C and vacuum ambient. All films were treated with essentially identical cure process conditions.

Refractive index and thickness were determined using a SCI FilmTek 2000 spectroscopic reflectometer. Electrical tests were performed using a mercury probe on low resistivity wafers ($< .02$ ohm-cm) of ≥ 450 nm film thickness. Mechanical properties were determined using an MTS model SA-2 nanoindentor on films greater than 500 nm thickness and according to manufacturer procedure for depth sampling. X-ray photoelectron spectroscopy (XPS) for atomic stoichiometry was collected in high resolution mode after Ar beam sputtering to remove a 100Å surface layer; analysis was performed either using a Kratos Axis NOVA XPS spectrometer or using a Physical Electronics 5000LS ESCA spectrometer. Transmission IR data were collected for films deposited on 8-12 ohm-cm substrates using a Thermo Nicolet 750 at 4 cm⁻¹ resolution with a nitrogen purged cell. Background contributions from the silicon substrate

[#] For the purposes of this paper, the term 'PDEMS films' designates those films which were deposited using a porogen precursor and an OSG matrix precursor, where the porogen is subsequently removed by UV treatment. The term 'DEMS films' designates those films which were deposited using only an OSG matrix precursor and UV post treatment was not used.

were subtracted for each IR spectrum, and the data were normalized to one micron thickness for comparison. Specular x-ray reflectivity (XRR) data were measured on a PANalytical MRD instrument with CuK α 1 radiation in a Θ -2 Θ , triple axis configuration. XRR data analysis was performed with PANalytical X'Pert Reflectivity software using film stoichiometry determined by

XPS and estimating hydrogen content. Positron annihilation lifetime spectroscopy (PALS) was performed at the University of Michigan [11, 12]. Depth profiles were collected using select positron beam energies of 0.55, 1.2, 3.2, and 4.2 keV, and spectra were fit assuming a spherical pore shape. Ellipsometric porosimetry (EP) was performed at SOPRA on their GES5 spectroscopic ellipsometer with toluene as the absorptive [13]. Total porosity and pore size distribution were calculated from the isotherm of toluene adsorption using Kelvin and Dubinin-Radushkevitch equations.

RESULTS

Film Properties

The materials properties and pore morphologies as determined by PALS and EP for PDEMS films produced from five different porogen precursors (aka. formulations) having dielectric constant values of $2.50 \pm .05$ are shown in Table I.

Table I. Film properties and morphology for five different PDEMS® ILD formulations relative to a DEMS® ILD film.

| Porogen Precursor | k | Modulus (GPa) | Density (g/cc) | Pore Diam * (nm) | Pore Diam ** (nm) | Interconnection Length (nm) * | % Porosity ** |
|-------------------|------|---------------|----------------|------------------|-------------------|-------------------------------|---------------|
| none | 3.20 | 17.7 | 1.42 | - | - | - | 0 |
| 1 | 2.49 | 6.6 | 1.11 | 1.27 | 1.8 | 40 | 30.5 |
| 2 | 2.46 | 7.8 | 1.18 | 1.30 | 1.8 | 30 | 29.8 |
| 3 | 2.48 | 7.1 | 1.16 | 1.66 | 1.8 | 5 | 24.3 |
| 4 | 2.49 | 7.9 | 1.16 | 1.34 | 1.4 | 35 | 27.7 |
| 5 | 2.53 | 10.8 | 1.25 | 1.30 | 1.6 | 25 | 29.0 |

* - PALS ** - EP

In order to test the hypothesis that pore size is related to the molecular volume of the porogen precursor, pore sizes determined from PALS and EP were compared to the molecular volume of the porogen precursor molecule estimated from its molecular weight and liquid density: $v = M/\rho$. The number of porogen precursor molecules per pore ranges from 4 to 10 by this estimation. These results do not correlate with the molecular volume of the porogen precursor or with the chemical nature of the porogen precursor (ie. degree of unsaturation[#], boiling point, etc...). In contrast, for a spin-on process, where the porogen may be introduced as a polymer or pre-made porogen, a relationship between porogen precursor volume and final pore size might be expected. Although there is no clear pore size trend for these CVD films, it can conclude that the pores must be formed by a species larger than one porogen precursor molecule. It is likely that the pores are due to clusters of molecules, which could be formed either in the plasma phase, on the film surface, or even in the bulk of the film during the cure stage (akin to an Ostwald Ripening effect).

[#] The degree of unsaturation of a hydrocarbon molecule is denoted as one half of the number of hydrogens that the molecule is deficient when compared to a fully saturated hydrocarbon as defined by the general empirical formula $C_nH_{(2n+2)}$.

The amount of porogen precursor needed in the reaction phase to introduce sufficient porosity into the post-treated film will depend on the ability of the porogen precursor or subsequent species produced in the film formation process to become incorporated into the film. For this study, the ratio of DEMS to porogen precursor varied from 3:2 to 1:4, where higher ratios were needed in cases where the relative reactivity of the porogen precursor is higher. The propensity of organic materials to react in a plasma and the rate of film formation has been studied and shown generally to be inversely related to the hydrogen yield from the molecule [14]. Reactivity in the plasma appears to be a necessary attribute of the porogen precursor, but not sufficient by itself to define an effective porogen precursor. The nature of the porogen material incorporated into the composite film has a significant impact upon the process conditions required to produce a porous film. It has been shown previously [10] for a given porogen precursor that a relationship exists between the concentration of the porogen precursor used in the formulation and the final porosity of the film. However, in general there appears to be little ability to alter pore size through variations in process conditions. Within the current sensitivity of pore size measurements pore size appears to be an inherent property of the porogen precursor. This suggests that the concentration of porogen precursor in the chemical feed affects mainly the number density of porogen species produced in the process and therefore the total porosity of the film, but has little effect upon the nature of the individual porogen species produced or the average pore size.

Film Structure and Dielectric Constant

A range of porosity values (24-31%) were determined by EP despite having similar dielectric constants for the various porous films. As process conditions did not vary significantly for the depositions (ie. the power density [14] was within $\pm 10\%$ of average for all depositions, the type of porogen precursor used appears to have a direct impact upon the formation of the OSG network. To understand the impact of porogen precursor type on the dielectric constant of the matrix, the infrared spectra and dielectric constants for PDEMS films from different porogen precursors were compared to that obtained for DEMS only films. The dielectric constant of a porous material is approximated by the Maxwell or Maxwell-Garnett [15] relationship for the case where the low dielectric constant phase is vacuum ($k=1$):

$$k_{porous} = \frac{c(1-\phi)k_{solid} + \phi}{c(1-\phi) + \phi} \quad (1)$$

where

$$c = \frac{2}{3} + \frac{1}{3k_{solid}} \quad (2)$$

k_{solid} is the dielectric constant of the solid phase, ϕ is the volume fraction of vacuum (aka. the porosity), and $(1-\phi)$ is the volume fraction of the OSG matrix. This equation has been found, by comparison to both experiment and finite-element simulations, to describe many porous materials reasonably well. Using the measured dielectric constant for the porous film, and porosity values determined by EP, the dielectric constant of the matrix of the porous films were calculated. In Figure 1 the calculated matrix dielectric constant is plotted against the integrated

IR area ratios of the Si-CH₃ species to the network area ratio[#]. Extrapolating Figure 1 to x=0 yields a dielectric constant value of 3.9, consistent with an undoped silica glass matrix. There is a range of dielectric constant determined for the matrices of various porous films that reflects the differing levels of porosity. Atomic compositions determined by XPS show close agreement between porous films with matrix dielectric constants determined to be ~ 3.2 and that of the DEMS® ILD film shown in Table I. It can be observed from Figure 1 that the matrix dielectric constants for the porous materials satisfy the same trend as the dense materials. These results indicate that the porogen precursor plays a role in modifying the deposition process and the dielectric constant of the OSG network deposited by this process.

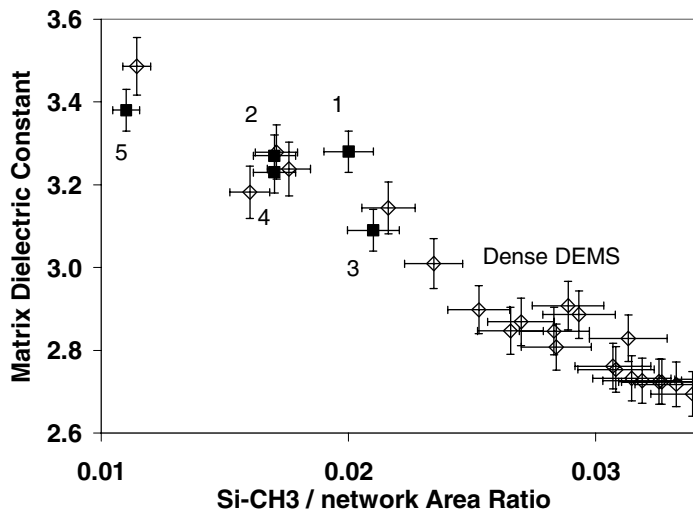


Figure 1. Calculated matrix dielectric constants for PDEMS films (solid squares) and measured dielectric constants for DEMS-only films (hollow circles) *versus* Si-CH₃ : network area ratios determined by FT-IR.

Film Structure and Mechanical Strength

It is well known that both degree of porosity and concentration of methyl groups impact the mechanical properties of organosilicate glasses [1,9,16]. The mechanical robustness of porous ILD films is one of the primary considerations in producing a material suitable for current BEOL interconnect schemes. We attempt to quantify the impact of both porosity and methyl group concentration on the observed diminution in mechanical properties, and show that porogen type can have a major impact upon the film properties.

Nanoindentation has arisen as the standard method of choice to provide surrogate tests of the mechanical strength of a film and its potential to withstand the rigors of integration. The agreement between mechanical properties determined by nanoindentation and EP ranged from less than 5% (Porogen 1, 5) to approximately 50% (Porogen 4). For the analysis shown here we exclusively use nanoindentation data to assess film property-composition/morphology trends.

In this study there was a wide range of film densities observed despite producing similar dielectric constant values. For PDEMS films the modulus determined by nanoindentation is linearly related to the film density determined by X-ray reflectivity, as shown in Figure 2. As

[#] The range of ~1300-1255 cm⁻¹ was used for the Si-CH₃ absorption, and in the range of 1255 – 975 cm⁻¹ for the network absorption. The integrated network area in the infrared is assumed to be primarily composed of various Si-O contributions [17].

shown previously, the film modulus, and therefore its density, are determined largely by the connectivity or methyl content of the network [1].

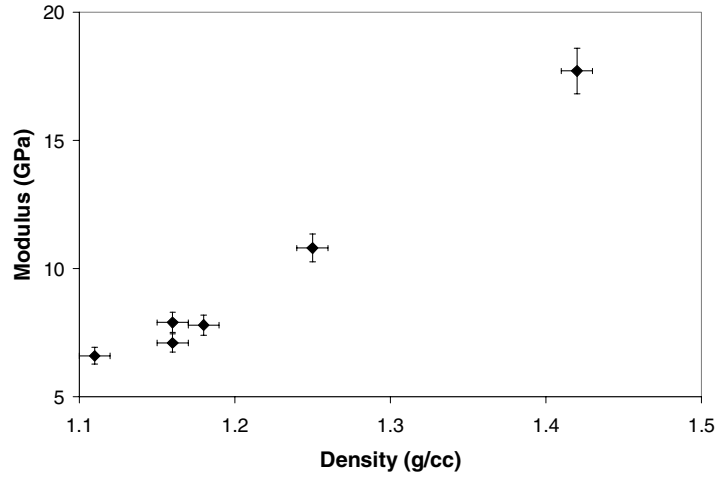


Figure 2. Mechanical properties *versus* density for DEMS and PDEMS films after UV cure.

The porosity dependence of modulus for many materials has been successfully modeled with simple power-law expressions: $E(\phi) = E(\phi=0) \cdot (1-\phi)^n$, where $2 < n < 4$ [17]. The glass-forming tendencies and mechanical properties of network solids in general have been described via “rigidity theory” [18]. In these and related works, the elastic modulus is related quantitatively to the average coordination number of the atoms in a solid; the more connected is the solid, the higher the mechanical properties. In a manner similar to Boolchand et al. [19] we derive a hardness index for doped silicates of formula SiO_yT_x where T is a terminal group such as $-\text{CH}_3$ and $y = 2-x/2$. The hardness index is given by the formula :

$$h = \frac{1 - \frac{3}{2}a \left(\frac{\text{Si} - \text{CH}_3}{\text{Network}} \right)}{1 + \frac{1}{2}a \left(\frac{\text{Si} - \text{CH}_3}{\text{Network}} \right)} \quad (3)$$

where $(\text{Si}-\text{CH}_3/\text{network})$ is the area ratio from FT-IR and a is a scaling factor to convert these area ratios to the actual ratios of methyl and oxygen species, respectively. In the idealized rigidity theory, there is a transition from soft materials to rigid materials as h rises above zero, or in this case as the methyl:oxygen ratio falls below $2/3$. A positive hardness index basically expresses an excess of bond stretching + bond bending constraints over the degrees of freedom of the network system. Boolchand et al. [19] suggest that the elastic modulus is proportional to h :

$$E(h) = E(h=1) \cdot h \text{ over the range } 0 \leq h \leq 1 \quad (4)$$

Combining this expression with that for the porosity dependence we find

$$E(\phi, h) = E_o \cdot h \cdot (1-\phi)^n, \text{ where } E_o = E(\phi=0, h=1) \quad (5)$$

captures the dependence of modulus on both porosity and the decreasing connectivity of the network as the concentration of terminal Si-CH₃ species rises.

Using a , n , and E_0 as flexible parameters the expression was fit to a series of data including numerous films produced from diethoxymethylsilane without porogen precursor and the 5 different porogen precursor formulations used in this study. The three lines for three different porosities shown in Figure 3 are all produced from the same set of parameters using equation 5. The data for the porous materials generally fall between the lines for 25% and 30% porosity which encompass their experimentally determined porosities. The resulting fit parameters are in reasonable agreement with values expected for these materials: E_0 of 56 GPa is in the range reported for CVD TEOS oxides, n of 3.6 is in the range found for other similar materials, and the a parameter (17.8) reasonably correlates the Si-CH₃/network ratios from FT-IR with atomic ratios for methyl groups and oxygen. Thus major trends in material modulus are captured by the simple combined expression which does not include secondary dependencies on other variables such as partial replacement of bridging oxygen with bridging methylene (eg. -CH₂-) groups. This data suggests that superior mechanical strength is obtained for porous films from matrices with higher matrix dielectric constant values (eg. reduced methyl concentrations). The mechanical properties for the porous materials are consistent with the network portion of the porous materials being very similar to the dense material, and this is consistent with similar observations on trends in dielectric constant mentioned previously.

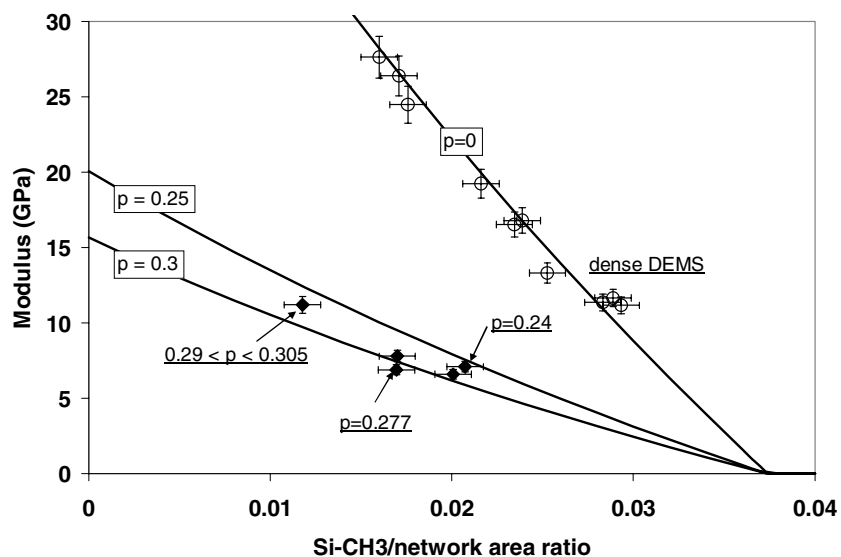


Figure 3. Measured modulus for PDEMS films (solid squares) and DEMS-only films (hollow circles) versus Si-CH₃: network area ratios determined by FT-IR. Lines correspond to different porosities as calculated from equation 5.

Molecular simulations were used to assess the expected impact of pore size on mechanical properties. An amorphous SiO₂ matrix was created via annealing of an initially random system of Si and O atoms in an approximately 2.5nm cube with periodic boundary conditions. This system was annealed in a series of constant temperature, constant pressure (NPT) molecular dynamics simulations. To study porous systems, either one or one or two roughly spherical pores were created in the matrix by removal of Si and O atoms, termination of any dangling bonds with hydrogen, and further annealing. Since the detailed structure of the amorphous

system varies by location, two arbitrary positions for the single pores were studied. Pore sizes introduced to the matrix were kept consistent with actual pore sizes observed in this study. A series of NPT molecular dynamics simulations were conducted at different isotropic pressures in order to determine the Bulk Modulus, which is reasonably proportional to Young's Modulus. To assess the impact of pore size, similar systems were created except they contained two pores instead of one.

Figure 4 shows that for this model the modulus decreases with porosity as $\sim (1-\phi)^5$ which is somewhat more rapid than most oxides with macro porosity and significantly faster than that predicted by the upper bound of Hashin-Shtrickmann theory [20]. The simulation indicates that there is no impact of pore location suggesting that the detailed local structure of the matrix is not critical. It also indicates that replacing one pore with two smaller pores shows no change in the relationship between modulus and porosity. This provides evidence that pore size at these dimensions is not expected to greatly impact the mechanical properties of the film, consistent with effective medium theories. This is in agreement with experimental evidence which does not indicate any systematic trend in the measured modulus of the films with pore size.

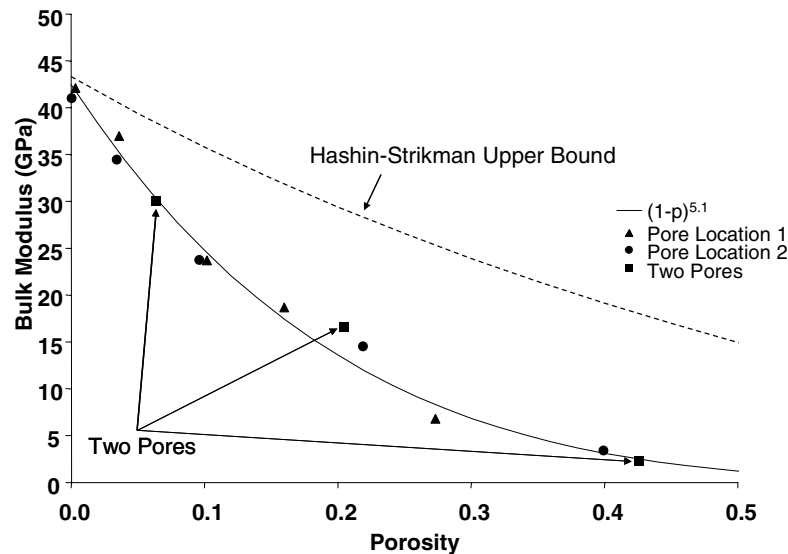


Figure 4. Molecular dynamics simulations of the effect of porosity and pore size on modulus.

Pore size and Interconnectivity

The relationships between pore size, total porosity, and pore interconnectivity are important for understanding the morphology of porous materials and how they interact with BEOL processes. By increasing the amount of a discrete minority phase in a continuum, the volume fraction of the minority phase will eventually reach a certain threshold number density such that percolation is reached. It is assumed that this phenomenon holds true for PDEMS films where pore interconnectivity has implications towards compatibility with subsequent processing steps.

For many kinds of two-phase systems the percolation threshold occurs near $\phi \sim 0.16$ [21]. The system of sticky or adhesive spheres is well-studied [22] and exhibits percolation thresholds which satisfy $\sim 0.1 < \phi_c < \sim 0.2$, depending on the value of a “stickiness” parameter. A percolation threshold value of ~ 0.2 was determined experimentally for thermodynamically phase-separated spin-on low k materials [23]. For impenetrable spherical inclusions in an ideal

continuous matrix the maximum possible threshold is the volume fraction of a closest-packed lattice (CPL), $\phi_c = 0.7405$. Here we model the limit of disconnected porosity for our systems by considering pores arranged in a CPL and taking into account a minimum separation between spheres which is set by physical and chemical properties of silicates. The wall thickness to pore diameter ratio is set by the basic geometrical expressions:

$$\phi = \phi_{\max} \left(\frac{1}{1 + t/D} \right)^3 \quad (6)$$

$$t/D = \left(\phi_{\max}/\phi \right)^{1/3} - 1 \quad (7)$$

where t and D are as shown in Figure 5, and $\phi_{\max}=0.7405$ (eg. where $t=0$ for a CPL). Equation 7 gives porosity as a function of t/D and we can further relate porosity to dielectric constant using the Maxwell relationship (eqn. 5). In Figure 6 we plot dielectric constant as a function of t for three different pore diameters (0.5, 1.0, 2.0 nm) assuming a matrix dielectric constant, $k_{\text{solid}} = 3.2$. In the figure, systems with a dielectric constant above a given line may have isolated pores, while those below the line would be expected to show interconnectivity. The point at which this occurs can be calculated for this system assuming the minimal wall thickness possible for an intact physical barrier between pores to be in the range of 0.5 nm (eg. the dimensions of a SiO_4 tetrahedral structure) to 0.6nm (eg. the width of a double-six-ring cage in the zeolite faujasite).

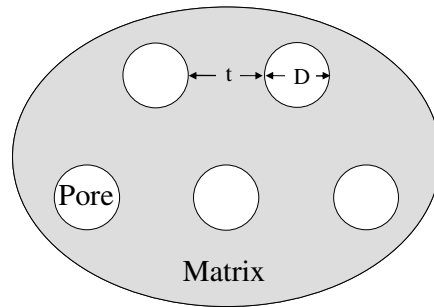


Figure 5. Pictorial description of dimensions used for equations 6 & 7

It can be clearly seen from Figure 6 how strongly the percolation threshold depends upon pore size for this model. For different pore sizes the plot defines the point at which a minimum given wall thickness (t) can be sustained; above each curve the porosity can be maintained without breaching a given minimum wall thickness. For a pore 2 nm in diameter the model predicts that pores could remain discrete up to a pore volume fraction of about 0.38 when $t=0.5$ nm. This corresponds to a porous film with a dielectric constant close to 2.2 having a matrix dielectric constant of 3.2. For pores 1 nm diameter the transition is reached at much lower pore volume fractions, around 0.22. This is a manifestation of the relationship that pore volume has with pore size; volume is proportional to the cube of the pore radius and for a given porosity so that the number density of pores increases by a factor of 8 when the pore size is reduced by half.

The model therefore suggests that even when pores are arranged on a CPL, which is the configuration that will produce the highest degree of discrete porosity, that interconnections

between pores will be observed at volume fractions exceeding only ~ 0.3 for typical pore sizes found in this study. The analysis of pore morphology using this model indicates that for a fixed dielectric constant, increasingly smaller pore dimensions lead to a transition from discretely dispersed pores within an OSG continuum (cf. Swiss cheese) to a homogeneous, low-density OSG matrix (cf. steel wool).

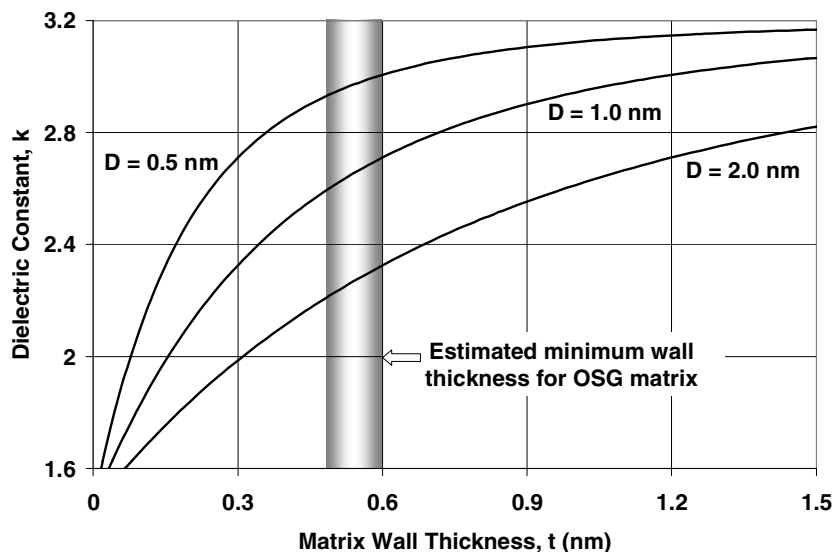


Figure 6. Modeling of percolation threshold for porous organosilicate glasses

The experimental data from PDEMS films shows average pore interconnection length that depends on both pore size and total porosity (Figure 7). As percent porosity increases from 24 to 30.5%, the average pore interconnectivity determined by PALS also increases from 5 to 40 nm. This is expected behavior; as the number density of pores increases the pores will be closer in proximity.

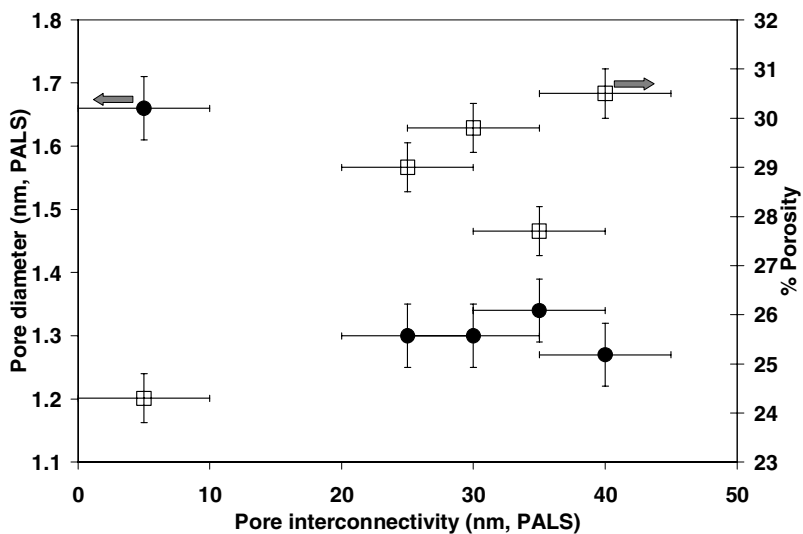


Figure 7. Pore size and porosity versus interconnection length determined by PALS

Figure 7 also plots mean pore size determined by PALS as a function of average pore interconnectivity. As predicted in the previous paragraph, the interconnectivity between pores is larger for a smaller pore size. It is important to note, however, that pore size and total porosity are changing at the same time for these PDEMS films, therefore it is difficult to separate the two effects and their contributions to interconnectivity.

We find the PALS and EP data to be very complimentary. For example, PALS is able to provide a measure of film uniformity with depth whereas EP is capable of providing quantitative measures of total porosity. Samples tested in this study showed very uniform depth profiles as indicated by uniform density depth profiles by XRR, pore size and positronium formation with depth of implantation, and film composition by dynamic SIMS. The consistency between porosities determined by EP and film property analysis suggests that the toluene probe used for EP provides an accurate measure of porosity in these films. However, the PALS method measures interconnectivity lengths on the order of nanometers. It is unclear whether there is significant permeability by the toluene probe used in the EP experiments through the thin OSG walls produced in these structures. The presence of interconnected pores in the film is not inconsistent with PALS data which provides an effective distance measurement for half of the implanted positronium to effectively diffuse out of the film. Even for PALS interconnectivity values of as low as 5 nm there was still observed measurable positronium escaping to vacuum from depths of over 100nm. The measure of interconnectivity provided by PALS may reflect the degree of tortuousness of the film's pore morphology rather than the actual pore interconnectivity. Based on the data it is expected that these films have some measure of interconnected pores at dielectric constants of 2.5.

CONCLUSIONS

Porous OSG materials produced by the PDEMS™ ILD process [4,9] are the leading candidates for back-end-of-line dielectric insulators for 45nm generation IC manufacturing and beyond. In this paper the impact of porogen precursor type on film properties, porosity, and pore size and morphology are examined. The porogen precursor can be used to tailor pore size; perhaps more unexpectedly, it also plays a role in the structure of the OSG network produced. The result is that porous films with similar dielectric constant values can be produced with varied mechanical properties and pore morphologies. The type of porogen precursor is found to have a significant impact on the methyl content of the OSG network. For a given dielectric constant it is possible to minimize the porosity by reducing the dielectric constant of the matrix for the porous films; these same factors, however, also appear to negatively impact the mechanical strength of the film. Pore size and porosity, and therefore methyl content of the OSG network, are the major factors affecting the interconnectivity of pores in these materials. At a fixed dielectric constant, minimizing the porosity and maximizing pore size are means by which pore interconnectivity can be minimized. Understanding the significance of pore morphology will be critical for successful optimization and integration of porous OSG materials for steps for back-end-of-line IC manufacturing.

ACKNOWLEDGEMENTS

The authors wish to thank David Gidley, H.-G. Peng and R.S. Vallery of the University of Michigan for PALS data and discussions; Adrien Darragon and Gary Brake of SOPRA for EP data and discussions. We also wish to thank P. McDaniel, X. Gao, J. Higgins, and C. Coe of our Corporate Research Services Department for their dedication to producing high quality materials

characterization information, Air Products – Carlsbad for support through chemical supply, and to Air Products management for permission to publish this work.

REFERENCES

1. M.L. O'Neill, R.N. Vrtis, J.L. Vincent, A.S. Lukas, E.J. Karwacki, B.K. Peterson, M.D. Bitner, MRS Symposium Proceedings **766**, 321 (2003)
2. G.Y. Lee, D.C. Edelstein, D. Dobuzinsky, G. Feng, K. Dev, K.-S. Low, P. Shafer, P. Wrschka, R. Conti, R. Schutz, W. Cote, *198th Annual Electrochemical Society Meeting*, **H-1** #531 (2000)
3. M.L. O'Neill, A.S. Lukas, R.N. Vrtis, J.L. Vincent, B.K. Peterson, M.D. Bitner, and E.J. Karwacki, *Semiconductor International* **25**(6), 93 (2002)
4. J.L. Vincent, M.L. O'Neill, H.P. Withers, S.E. Beck, R.N. Vrtis, U.S. Patent # 6,583,048 (24 June 2003)
5. N. Matsuki, Y. Naito, Y. Morisada, A. Matsunoshita, U.S. Patent # 6,352,945 (5 March 2002)
6. P.A. Van Cleemput, R.K. Laxman, J. Shu, M. Schulberg, B. Nie, U.S. Patent # 6,340,628 (22 January 2002)
7. D. Cheung, W-F. Yau, R.P. Mandal, S-P. Jeng, K-W Liu, Y-C Lu, M. Barnes, R.B. Willecke, F. Moghadam, T. Ishikawa, T.W. Poon, U.S. Patent #6,348,725 (19 February 2002)
8. M.L. O'Neill, A.S. Lukas, R.N. Vrtis, M.D. Bitner, E.J. Karwacki, J.L. Vincent, B.K. Peterson, presented at the 2003 American Vacuum Society National Meeting, Baltimore, MD (2003), unpublished
9. R.N. Vrtis, M.L. O'Neill, J.L. Vincent, A.S. Lukas, M. Xiao, J.A.T. Norman, U.S. Patent # 6,846,515 (25 January 2005)
10. R.N. Vrtis, M.L. O'Neill, J.L. Vincent, A.S. Lukas, B.K. Peterson, M.D. Bitner, E.J. Karwacki, MRS Symposium Proceedings **766**, 259 (2003)
11. D.W. Gidley, H.-G. Peng, R.S. Vallery, *Annu. Rev. Mater. Res.* **36**, 49 (2006)
12. D.W. Gidley, K.G. Lynn, M.P. Petkov, M.H. Weber, J.N. Sun, A.F. Lee, in *New Direction in Antimatter Chemistry and Physics* (Kluwer Acad. Pub. 2001) p. 151
13. M.R. Baklanov, K.P. Mogilnikov, *Microelectronic Eng.* **64**, 335 (2002)
14. Y. Yasuda, *Plasma Polymerization* (Academic Press, Orlando, Florida, 1985)
15. W. D. Kingery, *Introduction to Ceramics*, 2nd ed. (Wiley, New York, 1976); *Phil. Trans. R. Soc. Lond.* **203**, 385 (1904)
16. A. Grill, D.A. Neumayer, *J. App. Phys.*, **94**(10), 6697 (2003)
17. R.G. Munro, *Journal of Research of the National Institute of Standards and Technology*, **109**, 497 (2004)
18. Various references in *Rigidity Theory and Applications*, edited by M.F. Thorpe, P.M. Duxbury, (Kluwer Academic, New York, 1999)
19. P. Boolchand, M. Zhang, B. Goodman, *Phys. Rev. B*, **53**, 11488 (1995)
20. Z. Hashin, S. Shtrikman, *J. Mech. Phys. Solids*, **11**, 127 (1963)
21. H. Scher, R.J. Zallen, *J. Chem. Phys.*, **53**, 3759 (1970)
22. S. Torquato, *Random Heterogeneous Materials*, (Springer, New York, 2002)
23. R.D. Miller, R. Beyers, K.R. carter, R.F. Cook, M. Harbison, C.J. Hawker, J.L. Hedrick, V. Lee, E. Liniger, C. Nguyen, J. Remenar, M. Sherwood, M. Trollsas, W. Volksen, D.Y. Yoon, MRS Symposium Proceedings **565**, 3 (1999)